

HIGHER ORDER GEOMETRICAL DISTORTION IN SERIAL MR BRAIN IMAGES

Mark Holden¹, Marcel Breeuwer², Kate McKleish¹, David J. Hawkes¹, Stephen Keevil¹ and Derek L. G. Hill¹

¹Radiological Sciences and Medical Engineering, GKT School of Medicine, 5th Floor Thomas Guy House, Guy's Hospital, London SE1 9RT, United Kingdom.

²Philips Medical Systems, EasyVision Advanced Development, Building QV1, P.O. Box 10.000, 5680 DA Best, The Netherlands.

1 - Introduction

Geometrical distortion leads to inter-acquisition geometrical change that impedes the detection of clinically interesting anatomical change. Geometrical distortion arises from incorrect frequency encoding because of: (1) imaging gradients errors; (2) B_0 inhomogeneities; (3) chemical shift artefact; (4) object susceptibility changes. Susceptibility and chemical shift effects can be reduced by increasing the readout gradient strength. Previous work on geometrical distortion for serial MR studies has focused on scaling error. Here we use a new 3D phantom and distortion detection software to investigate more general orders described by a 4th-order polynomial. Our aim is to quantify distortion up to 4th-order caused by hardware limitations under normal use and identify the factors that lead to distortion change so we can accurately correct distortion in serial MR brain images. Accordingly, we have designed a set of experiments to assess the impact of various sequence parameters.

2.1 - Theory: sources of distortion

$$s(t) = \int \rho(\mathbf{x}, \sigma_{cs}) e^{-j\gamma t [\phi(G_x) + \Delta\phi(G_x, B_e, \sigma_{cs}, \chi)]} d\mathbf{x}$$

Where $G_x'(\mathbf{x}, G_x)$ is the error in readout gradient G_x ; $B_e(\mathbf{x})$ is the error in B_0 ; $\sigma_{cs}(\mathbf{x})$ is the chemical shift shielding constant and $\chi(\mathbf{x})$ is the magnetic susceptibility.

$$\phi(G_x) = G_x x \quad (\text{no distortion})$$

$$\Delta\phi(G_x', B_e, \sigma_{cs}, \chi) = \underbrace{G_x' x + B_e}_{\text{scanner-dependent}} + \underbrace{\sigma_{cs} B_0 + B_0 f(\chi)}_{\text{object-dependent}} \quad (\text{distortion})$$

2.2 - Theory: measuring distortion

We model scanner-dependent distortion with a 4th-order 3D polynomial transformation \mathbf{T} :

$$\mathbf{x}' = \mathbf{T}(\mathbf{x}) = \mathbf{t} + \mathbf{A}\mathbf{x} + \mathbf{B}\mathbf{x}^2 + \mathbf{C}\mathbf{x}^3 + \mathbf{D}\mathbf{x}^4 + \mathcal{O}(\mathbf{x}^5)$$

Where $\mathbf{x}' = (u, v, w)^T$ is a point in the distorted space \mathbf{X}' (\mathbf{t} = transpose), $\mathbf{x} = (x, y, z)^T$ is a point in the undistorted reference space \mathbf{X} ; $\mathbf{x}^2 = (xy, xz, yz, x^2, y^2, z^2)^T$ is a vector containing the 2nd-order terms, \mathbf{x}^3 and \mathbf{x}^4 are vectors containing the 3rd- and 4th-order terms, \mathbf{t} is a translation vector, \mathbf{A} , \mathbf{B} , \mathbf{C} , \mathbf{D} are matrices containing the 1st-, 2nd-, 3rd- and 4th-order transform coefficients and $\mathcal{O}(\mathbf{x}^5)$ is the order 5 and higher terms (which are neglected). \mathbf{A} , \mathbf{B} , \mathbf{C} , \mathbf{D} and \mathbf{t} are estimated by scanning a phantom that contains several hundred of reference structures on accurately manufactured positions, detecting these positions in the scanned images and registering the detected positions \mathbf{X}' to their corresponding ideal positions \mathbf{X} . The number of transform coefficients N to be estimated depends on the order of the transformation \mathbf{T} (see table below). The estimation of these coefficients amounts to solving an overdetermined set of linear equations. We use the well-known method of Singular Value Decomposition to solve this set. We estimate the total distortion

Model order	Transform parameters	Number of coefficients
1	\mathbf{t} (3 x 1) and \mathbf{A} (3 x 3)	12
2	\mathbf{t} , \mathbf{A} , and \mathbf{B} (3 x 6)	30
3	\mathbf{t} , \mathbf{A} , \mathbf{B} and \mathbf{C} (3 x 10)	60
4	\mathbf{t} , \mathbf{A} , \mathbf{B} , \mathbf{C} and \mathbf{D} (3 x 15)	105

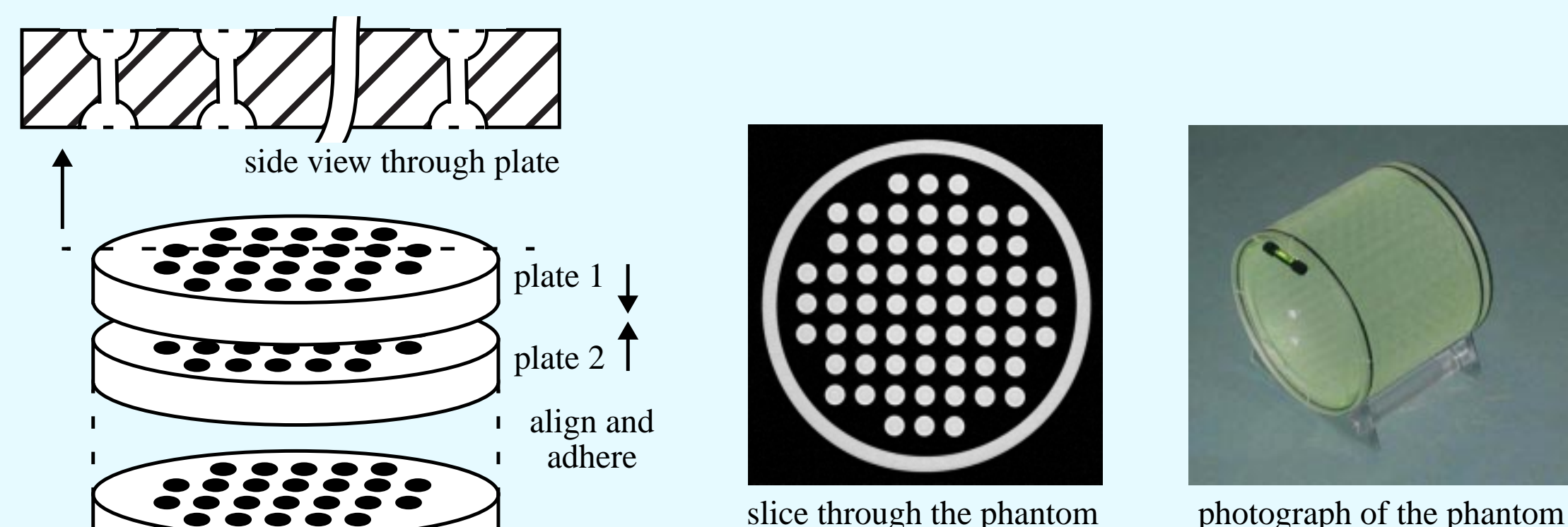
present with the dp residual, mean distance between \mathbf{X} and \mathbf{X}' , and the distortion for each polynomial order with the dp_4 four-tuple residual measure below:

$$dp_4 = \frac{1}{dp} [dp - dp(1), dp(1) - dp(2), dp(2) - dp(3), dp(3) - dp(4)]$$

$$\text{where } dp = \frac{1}{N} \sum_{\mathbf{x} \in \mathbf{X}, \mathbf{x}' \in \mathbf{X}'} |\mathbf{x} - \mathbf{x}'| \quad \text{and} \quad dp(i) = \frac{1}{N} \sum_{\mathbf{x} \in \mathbf{X}, \mathbf{x}' \in \mathbf{X}'} |\mathbf{T}_i \mathbf{x} - \mathbf{x}'|$$

3.1 - Method: 3D phantom design

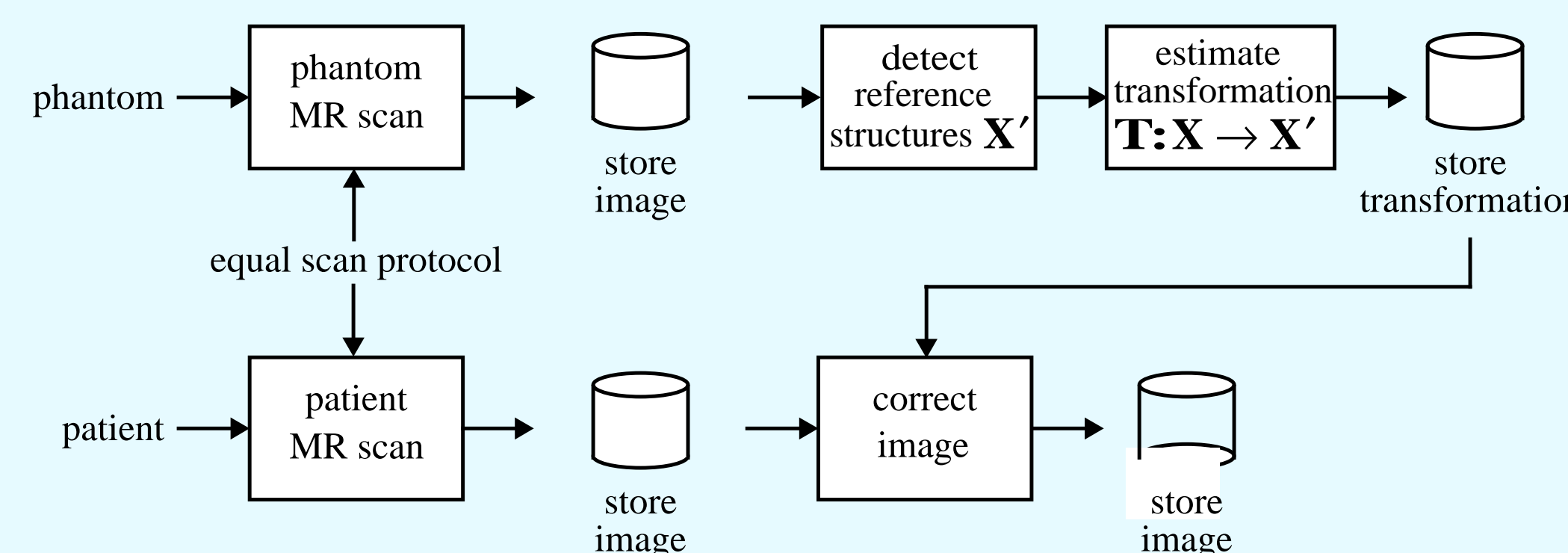
The phantom is built from acrylic plates with accurately (0.02mm) drilled hollow spheres, enclosed in a cylinder filled with copper sulphate solution - so forming a matrix 427 spheres, see below.



Acrylic plates with holes drilled to create the reference structures. Plates are then aligned and bonded together.

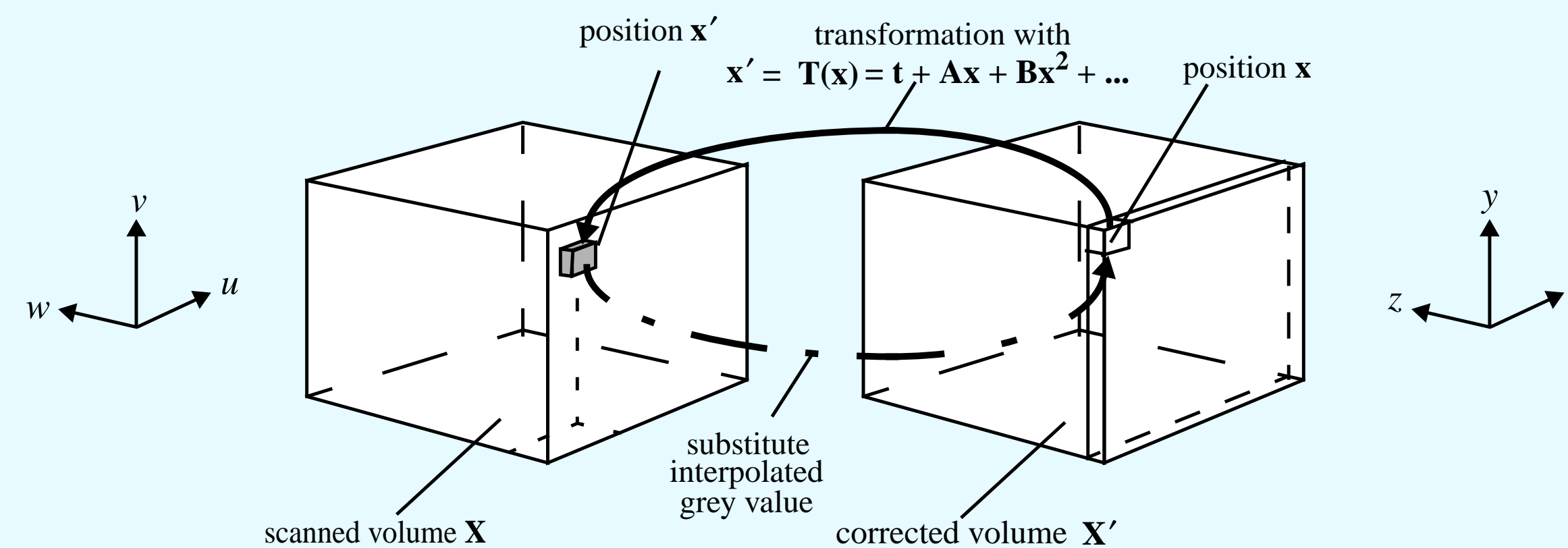
3.2 - Method: measuring and correcting distortion

Patient and phantom are scanned using the same MR sequence parameters. The centres of reference structures are detected using conditional erosion/dilation and C.O.G. operators. Then the polynomial transformation, \mathbf{T} , is determined by point-based registration (SVD) of the set of distorted points (\mathbf{X}') with the points corresponding to the manufactured sphere centres (\mathbf{X}).



3.3 - Method: correction of patient images

Once \mathbf{T} is known, patient images can be corrected. For every voxel position $\mathbf{x} \in \mathbf{X}$, the corresponding position $\mathbf{x}' \in \mathbf{X}'$ is calculated from the estimated transformation, $\mathbf{T}: \mathbf{X} \rightarrow \mathbf{X}'$. The intensity of the voxel at position \mathbf{x} is then interpolated from the voxels in the neighbourhood of \mathbf{x}' using either a sinc or tri-linear interpolation kernel as shown below:



3.4 - Method: experiments

We acquired $n > 30$ standard 3D gradient echo (FFE) and multi-slice spin echo (SE) image sets of the phantom with a Philips Gyroscan ACS2 1.5T MR scanner at two resolutions with the following sequence parameters. FFE1: voxel size 1x1x1.8mm, 256mm FOV, 124 slices, $G_x = 2.55\text{mT/m}$. FFE2: voxel size 2x2x2mm, 256mm FOV, 110 slices, $G_x = 1.275\text{mT/m}$. For both FFE1 and FFE2, TR/TE/flip angle were 30/4.5/30. SE: voxel size 2x2x2mm, 256mm FOV, 110 slices, $G_x = 1.275\text{mT/m}$, TR/TE = 500/20ms. For all scans the readout gradient was in the A/P direction. We measured distortion either with respect to physical space or relative to another phantom scan. We describe linear distortion by: scale (s_x, s_y, s_z) and shear (s_{xy}, s_{xz}, s_{yz}) components, and higher order distortion by polynomial coefficients; using the coordinate system: $x \leftrightarrow \text{A/P}$, $y \leftrightarrow \text{L/R}$, $z \leftrightarrow \text{H/F}$

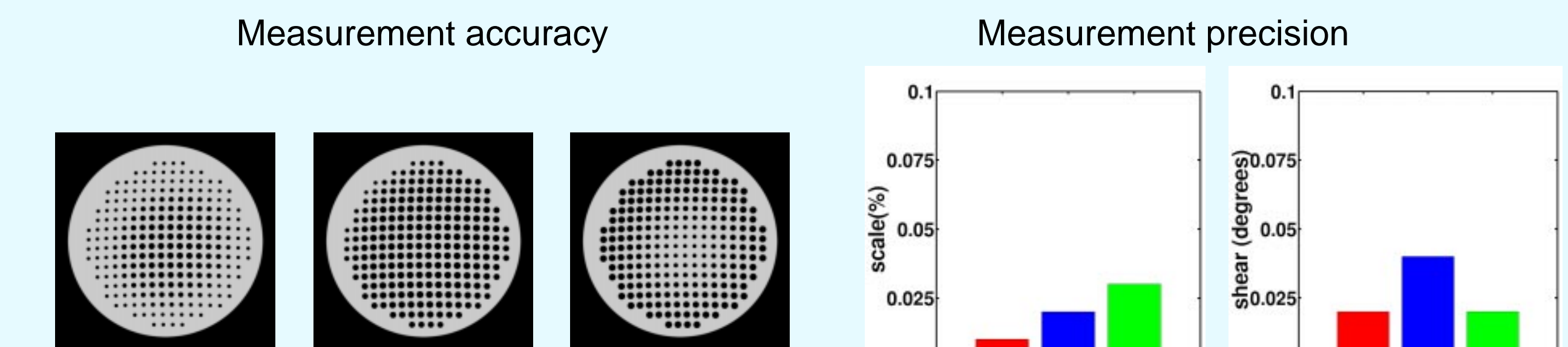
We measured the accuracy of distortion detection with synthetic phantom images containing known amounts of distortion and the precision with six consecutive FFE1 scans with repositioning and calculated the standard deviation of the 6 components of linear distortion.

We investigated the impact of the readout gradient strength, G_x , with six FFE2 scans with G_x ranging from 0.64 to 1.75mT/m.

The influence of the sequence parameters was studied by varying TR, TE, flip angle and the slice gap to produce five FFE2 and five SE scans that differed by one parameter from the baseline. Shim settings were investigated with three FFE1 and three FFE2 scans that differed only in shim setting: default shim (DS), auto shim (AS) and manual shim (MS). DS refers to the shim that was set at installation and optimised over the scanner's imaging volume; AS refers to automatic shimming immediately prior to scanning and was optimised over the FOV; and MS to volume-localised shimming over a 1cm³ volume at the phantom's centre, performed using the spectroscopy package. We estimated the total amount of distortion using the dp residual and amount of distortion for each polynomial order with the dp_4 residual.

To measure the distortion as a function of time we measured the change in distortion with respect to the first for a series of 11 weekly FFE1 scans.

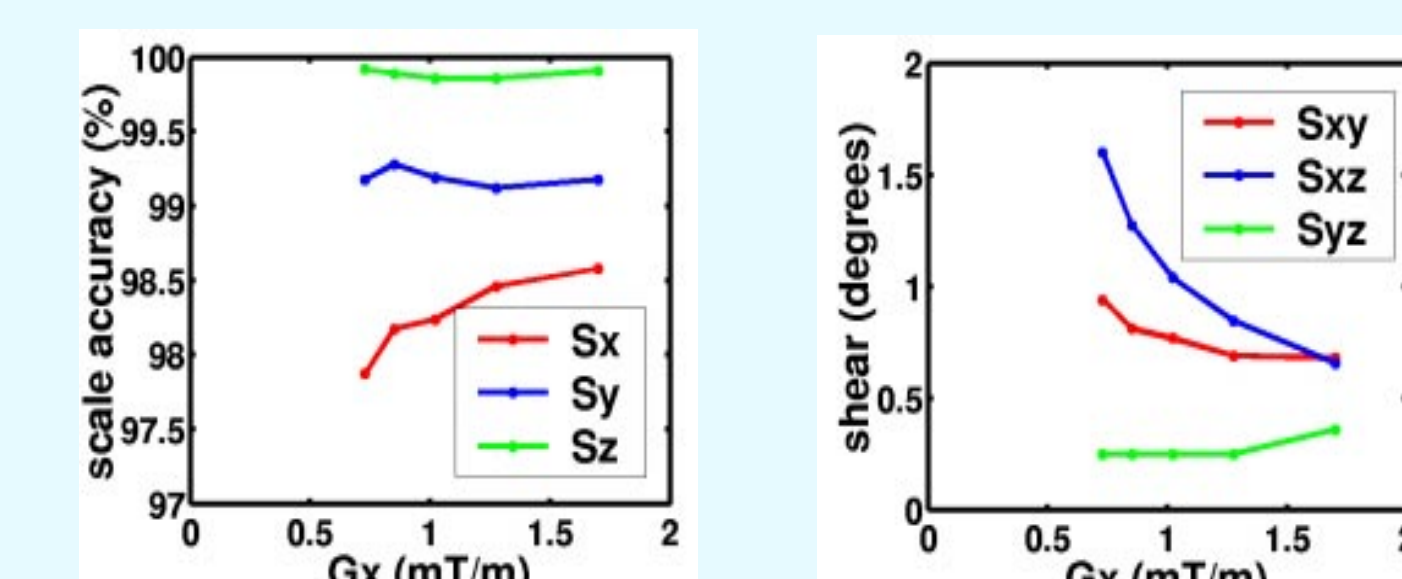
4 - Results



For the synthetic scans the transformation coefficients were determined to a mean relative error of < 1%. Shown are three consecutive slices through a synthetic image

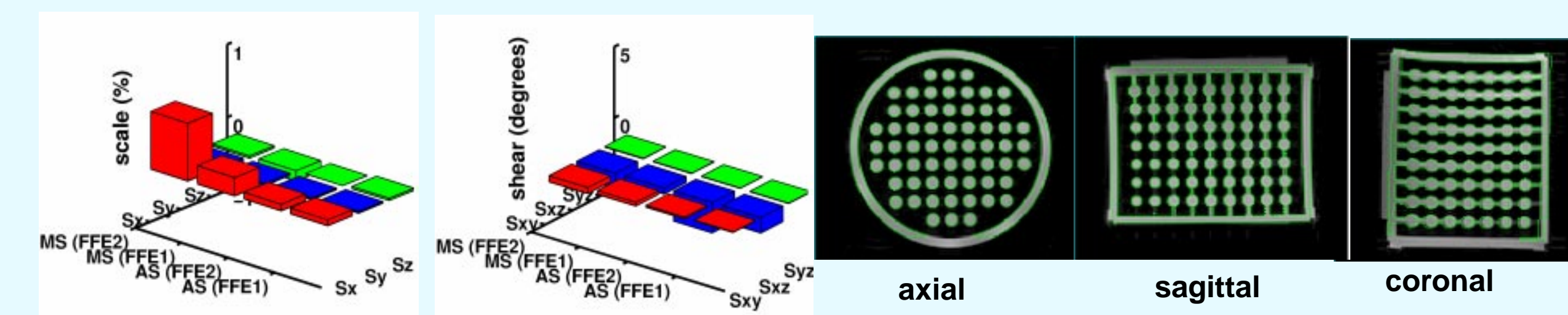
The precision (stdev) of the linear distortion terms for the six FFE2 scans was: (s_x, s_y, s_z) <= 0.03% and (s_{xy}, s_{xz}, s_{yz}) <= 0.04^o.

Readout gradient strength



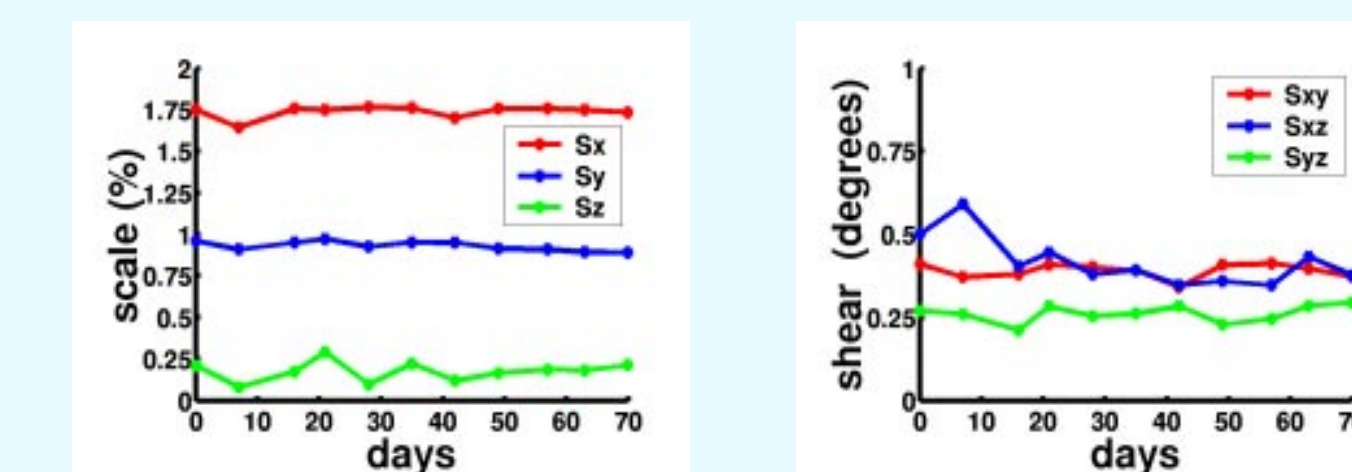
For distortion change as a function of G_x , the standard deviation of the ($s_x, s_y, s_z, s_{xy}, s_{xz}, s_{yz}$) components was (0.27%, 0.06%, 0.03%, 0.11^o, 0.37^o, 0.05^o) showing most change in the readout dependent directions (s_x, s_{xy}, s_{xz}). The coefficient of linear correlation, r , for (s_x, s_{xy}, s_{xz}) with decreasing, G_x , was (0.93, 0.87, 0.94) showing a high inverse linear correlation with G_x . The dp_4 residual was (32.94%, 39.61%, 5.60%, 1.88%) indicating that almost all the distortion change was either first or second order.

Shim setting



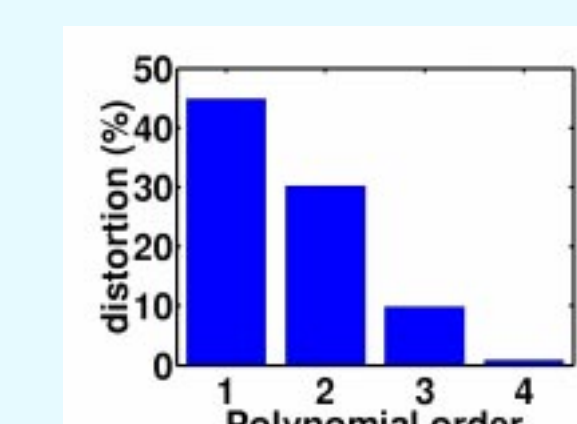
The largest distortion change for the FFE2 scans was for the AS and DS shim settings ($dp = 1.2\text{mm}$). The largest components for these settings were $s_x = 0.08\%$, $s_{xz} = -1.09^o$ for FFE1 which increased to $s_x = 0.09\%$, $s_{xz} = -2.13^o$ for FFE2. There was a similar pattern of increase for the MS to DS correction: $s_x = 0.25\%$, $s_{xz} = -0.43^o$ for FFE1 $s_x = 0.78\%$, $s_{xz} = -1.11^o$ for FFE2. Shim changes introduced a near linear distortion change: $dp_4 = (71.93\%, 0.00\%, 0.00\%, 0.00\%)$ (FFE1, AS to DS); $dp_4 = (54.29\%, 0.00\%, 0.00\%, 2.86\%)$ (FFE1, MS to DS). For the various sequence parameters the largest components of linear distortion were also (s_x, s_{xy}, s_{xz}). The mean (stdev) for (s_x, s_{xy}, s_{xz}) for both sequences was - FFE2: $s_x -1.53$ (0.28), $s_{xy} 0.60$ (0.07), $s_{xz} 0.92$ (0.21); SE: $s_x -1.35$ (0.82), $s_{xy} 0.40$ (0.21), $s_{xz} -2.41$ (0.92). The sagittal shear, s_{xz} , was significantly higher for SE than for FFE2 ($p < 0.01$).

Distortion as a function of time



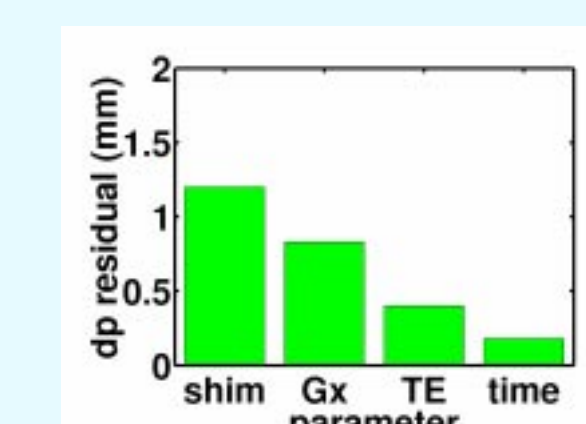
For the time series of 11 weekly scans, mean (stdev) 7 (1) days, the standard deviation of the distortion components ($s_x, s_y, s_z, s_{xy}, s_{xz}, s_{yz}$) was (0.09%, 0.04%, 0.06%, 0.02^o, 0.05^o, 0.03^o).

Polynomial order of distortion



For the set of 33 FFE1, FFE2 and SE scans, corrected to physical space, the mean residual, dp , decreased as a function of the order of correction ($r = 0.9$, $n = 33$). The mean ($n = 33$) dp_4 measure was (44.83%, 30.16%, 9.85%, 0.9%) indicating that 75% of the distortion was either first or 2nd-order.

Comparison of sources of distortion



Changes in the shim setting (AS/DS) produced the largest change, $dp = 1.2\text{mm}$. Changes in G_x resulted in $dp = 0.8\text{mm}$. Reducing TE from 4.5 to 3 msec resulted in $dp = 0.4\text{mm}$, and the changes over 11 weeks corresponded to $dp = 0.2\text{mm}$

5 - Discussion

We have shown high distortion measurement accuracy (coefficient error < 1%) with synthetic images and high precision (scale <= 0.03%, shear <= 0.04^o) with MR scans. Distortion in the readout dependent directions increased with decreased readout gradient strength, G_x , ($r > 0.93$) - consistent with theory. Changes in G_x led to 1st- and 2nd-order distortion changes, but not 3rd- and 4th-order ones. Scanner distortion may be smaller for 3D gradient echo (FFE) scans than 2D multi-slice spin echo ones possibly because of distortion introduced by slice selection. Distortion change over 11 weeks was: scale < 0.1%, shear <= 0.05^o which is negligible for clinical serial MR. Different shims produced only linear distortion changes. The largest distortion change for 3D gradient echo scans (FFE1) was for the autoshim and default shims which led to a shear change > 1^o.

References

- [Breeuwer] SPIE Medical Imaging Vol. 4322, 2001.
- [Hajnal] JCAT 19(5), p. 677-691, 1995.
- [Holden] Proc. SPIE Medical Imaging Vol. 4322, 2001 and Vol. 3661, pp. 44-55, 1999.
- [Lemieux] Medical Physics, 25(6), pp. 1049-1054, 1998.